ChemComm

Accepted Manuscript

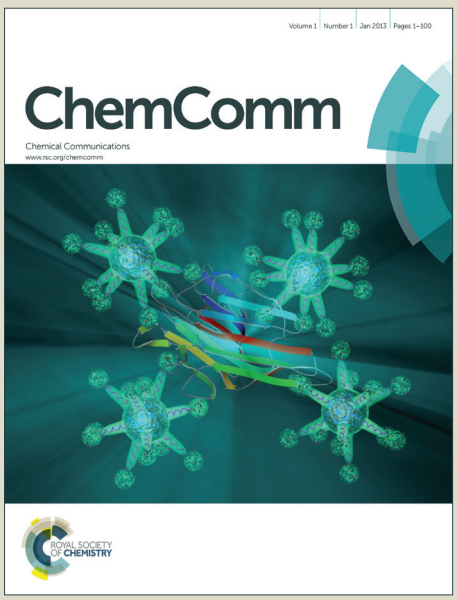

ROYAL SOCIETY OF CHEMISTRY

www.rsc.org/chemcomm

Journal Name

RSCPublishing

COMMUNICATION

Site-Specific Dynamics of Amyloid Formation and Fibrillar Configuration of $A\beta_{1-23}$ Using an Unnatural Amino Acid

Cite this: DOI: 10.1039/xoxxoooooox

Received ooth January 2012,
Accepted ooth January 2012

DOI: 10.1039/xoxxoooooox

www.rsc.org/

Haiyang Liu,[a] Richard Lantz,[a] Patrick Cosme,[a] Nelson Rivera,[b] Carlos Andino,[b] Walter G. Gonzalez,[c] Andrew C. Terentis,[a] Ewa P. Wojcikiewicz,[d] Rolando Oyola,[b] Jaroslava Miksovska[c] and Deguo Du*[a]

We identify distinct site-specific dynamics over the time course of $A\beta_{1-23}$ amyloid formation by using an unnatural amino acid, *p*-cyanophenylalanine, as a sensitive fluorescent and Raman probe. Our results also suggest the key role of an edge-to-face aromatic interaction in the conformational conversion to form and stabilize β-sheet structure.

Progression of protein anomalous misfolding and aggregation events that form amyloid fibrils is closely related to a number of amyloid diseases, such as Alzheimer's and Parkinson's diseases.[1] Amyloid fibrils normally contain a cross-β-sheet architechture extending in a direction parallel to the fibril axis.[2] However, the mechanistic view of protein self-assembly to form amyloids is still not fully understood, partly due to very limited experimental means to examine the dynamic details of protein aggregation in real time. This dramatically hinders the efforts for understanding of the mechanisms of protein amyloidogenesis and the pathogenic nature of amyloid fibrils. Moreover, an accumulating body of recent evidence suggests that the diffusible intermediate assemblies appear to be key species on the aggregation pathway and are engaged in the pathology of amyloid diseases.[3] This highlights the importance of elucidating high-resolution dynamics along aggregation pathways, e.g., aggregation dynamics at residue-specific level, for a comprehensive understanding of the molecular basis of amyloid diseases.

Extrinsic fluorescent dyes have been commonly used for probing conformational changes in protein self-assembly.[4] Recently, an unnatural amino acid, *p*-cyanophenylalanine (Phe_{CN}) (Fig. 1A), has received a great deal of attention as a usfeul spectroscopic reporter of protein structure and dynamics,[5] because of the optical sensitivity of its CN group to specific characteristics of local environment. The fluorescence quantum yield of Phe_{CN} decreases upon dehydration, making it a sensitive fluorescent probe of local hydrophobic environment.[5c-f] The CN streching frequency is highly sensitive to the electric field in its environment[6] and solvent polarity,[7] thus making the cyano moiety also a sensitive vibrational probe. Moreover, substitution of natural amino acids, such as Phe and Tyr, with Phe_{CN} introduces little structural perturbation because of their structural similarity. Recently, Phe_{CN} has been widely used as a site-specfic spectroscopic reporter of protein folding dynamics,[5f, 8] but so far it has seen very limited application of this probe in studies of protein self-assembly and amyloid formation.[9] The utility of this probe for distinguishing local dynamics along protein aggregation remains to be further explored.

Herein, using Phe_{CN} as a molecular probe, we clarify distinct and residue-specific dynamics along the aggregation pathway of an $A\beta_{1-23}$ peptide. $A\beta_{1-23}$ is the N-terminal fragment of the $A\beta_{1-40}$ peptide (Fig. 1A), which is the principal component of extracellular amyloid plaques accumulated in Alzheimer's disease. Peptide fragments were found to form fibrillar structures that resemble the biochemical and structural nature of amyloids formed by much larger proteins. Thus peptide fragments, especially from key regions of disease-related amyloidogenic proteins, have been extensively studied for understanding the nature of protein amyloid formation.[10] This approach reduces the complexity of the system for investigating the detailed mechanistic dynamics of aggregation. Here, specifically, in spite of its relatively short sequence, $A\beta_{1-23}$ contains the crucial amino acid region of $A\beta_{1-40}$ including the critical central hydrophobic cluster "LVFFA", and to our knowledge, has not been widely studied previously. We envision that it may represent a valuable model molecule for both experimental and computational studies of the mechanism(s) of protein amyloidogenesis. In addition, all of the aromatic Tyr and Phe residues in $A\beta_{1-40}$ are present in the $A\beta_{1-23}$ sequence. In the present work, Tyr10, Phe19, Phe20, and Phe4 residues in $A\beta_{1-23}$ were substituted to Phe_{CN}, respectively, to make four mutants $A\beta_{1-23}$M1-M4 (Fig. 1A).

We first investigated the aggregation of $A\beta_{1-23}$ via a thioflavin T (ThT) fluorescence assay using a fluorescence plate reader. The aggregation kinetics of $A\beta_{1-23}$ display a typical sigmoidal curve expected for amyloid formation, with a lag phase shortened upon increase of peptide concentration (Fig. 1B). The aggregation-induced secondary structure change from random coil to β-sheet structure was monitored by circular dichroism (CD) spectroscopy (Fig. 1C). The formation of amyloid fibers was further confirmed by atomic force microscopy (AFM) imaging, with typically 7-10 nm in height and 0.4-1.5 μm in length fibers observed (Fig. 1D). These data illustrate that $A\beta_{1-23}$ peptide steadily aggregates presumably by a nucleated polymerization mechanism, mimicking that of the wild type $A\beta_{1-40}$ peptide.[11] The aggregation rate of $A\beta_{1-23}$ is also sensitive to environmental factors such as ionic strength, pH, temperature, and metal ions, as shown in Fig. S1-S4.

To gain insight into the β-sheet structural properties in $A\beta_{1-23}$ amyloids, we measured the attenuated total reflection FTIR (ATR-FTIR) spectra of the aggregates. The amide I′ region of the spectrum shows two characteristic bands centered at 1619 and 1683 cm^{-1} (Fig. S5), revealing the presence of antiparallel β-sheet structure in $A\beta_{1-23}$ amyloid fibrils.[12]

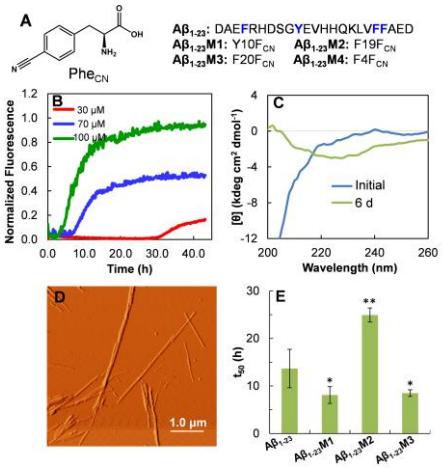

Fig. 1 (A) Structure of Phe_{CN} and the sequence of the wild type $A\beta_{1-23}$ peptide and the mutants. F_{CN} denotes Phe_{CN}. (B) Aggregation kinetics of $A\beta_{1-23}$ followed by ThT fluorescence. (C) CD spectra of $A\beta_{1-23}$ (100 μM) before and after 6 d of incubation. (D) AFM image of the $A\beta_{1-23}$ amyloid, acquired after incubating $A\beta_{1-23}$ (100 μM) for 6 d. (E) Comparison of half time (t_{50}) of the aggregation kinetics of $A\beta_{1-23}$ and the three mutants (70 μM). Asterisk (*) represents *P*-value > 0.05, and double-asterisk (**) represents *P*-value < 0.02.

Substitution of either Phe or Tyr to Phe_{CN} is expected not to have a dramatic effect on the aggregation properties because of their structual similarity. Indeed, our results show that the $A\beta_{1-23}$M1-M3 mutants all aggregate into amyloid fibrils. $A\beta_{1-23}$M1 and $A\beta_{1-23}$M3 aggregate with a slightly faster rate compared to that of the wild type $A\beta_{1-23}$ (Fig. 1E and Fig. S6), while a *P*-value of > 0.05 between the mean t_{50} values of the wild type peptide and the two mutants suggests that the difference of the aggregation rates is not significant (Fig. 1E). In contrast, $A\beta_{1-23}$M2 aggregates with a noticeably slower rate. The difference in their aggregation rates indicates the sensitivity of aggregation kinetics of such short peptides to even minimal side chain modification on certain residues. As shown in AFM images (Fig. S7), $A\beta_{1-23}$M1 and $A\beta_{1-23}$M3 formed fibrillar structures like that of native $A\beta_{1-23}$. $A\beta_{1-23}$M2 appeared to form shorter fibers, likely due to its slower aggregation rate. In addition, the appearance of two aggregation bands in infrared spectra of $A\beta_{1-23}$M1-M3 suggests the formation of antiparallel β-sheet structure in the amyloids (Fig. S5). A cross-seeding assay shows that the presence of preformed $A\beta_{1-23}$M1-M3 amyloid seeds significantly facilitated the aggregation rate of the wild type $A\beta_{1-23}$ peptide (Fig. S8), suggesting a compatible structural architecture of the amyloids of $A\beta_{1-23}$ and the mutants. Taken together, the results suggest that Phe_{CN} mutation at these amino acid positions does not change the fibrillar structural characteristics dramatically, while it may affect the aggregation energetics and therefore the kinetics of amyloid formation of $A\beta_{1-23}$. Surprisingly, substitution of Phe4 to Phe_{CN} dramatically interrupts peptide amyloidogenesis. There is negligible binding to ThT after 40 h of incubation of $A\beta_{1-23}$M4 (Fig. S6). No fibers were observed after 6 d of incubation (Fig. S7). The infrared spectrum of $A\beta_{1-23}$M4 after 4 d of incubation shows only a broad amide I′ band at 1645 cm^{-1}, characteristic for disordered structure (Fig. S5). These results strongly indicate the essential role of Phe4 side chain in determining the aggregation propensity of $A\beta_{1-23}$.

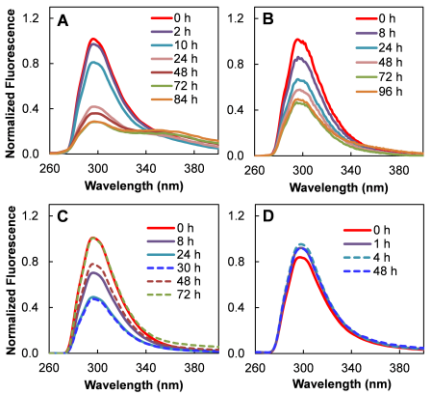

Fig. 2 Time-dependent Phe_{CN} fluorescence spectra of $A\beta_{1-23}$M1 (A), $A\beta_{1-23}$M2 (B), $A\beta_{1-23}$M3 (C) and $A\beta_{1-23}$M4 (D) peptides (100 μM).

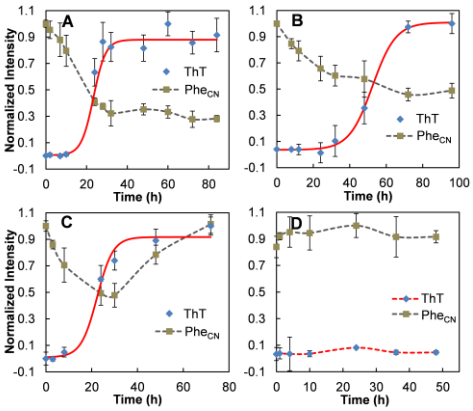

Fig. 3 Aggregation kinetics of $A\beta_{1-23}$M1 (A), $A\beta_{1-23}$M2 (B), $A\beta_{1-23}$M3 (C) and $A\beta_{1-23}$M4 (D) measured by Phe_{CN} fluorescence (square, intensity at 298 nm) and ThT binding fluorescence (diamond, intensity at 485 nm). Data are reported as means ± SD of triplicate results. The solid curves in A-C are fit of the ThT fluorescence to a sigmoidal equation. The other dashed curves are to guide the eye.

To reveal the local conformational dynamics along the aggregation pathway, the time-dependent Phe_{CN} fluorescence of the mutants was monitored, with the ThT-binding fluorescence measured in parallel. The fluorescence quantum yield of Phe_{CN} strongly depends on the properties of the local environment, e.g., the hydrophobicity of the surroundings.[5c, 9b, 13] As seen in Fig. 2 and 3, although the $A\beta_{1-23}$M1-M3 peptides all aggregate to form amyloids, the fluorescence intensity change of Phe_{CN} is highly dependent on its position in the primary sequence. The fluorescence intensity of Phe_{CN}10 in $A\beta_{1-23}$M1 shows a decrease over time, which starts prior to the onset of fibril formation, as depicted by ThT binding curve (Fig. 2A and 3A). The Phe_{CN}19 fluorescence intensity of $A\beta_{1-23}$M2 also decreases over time (Fig. 2B and 3B). Interestingly, for $A\beta_{1-23}$M3, the fluorescence intensity decreases in the first 30 h of incubation, overlapping largely with the ThT lag phase, and is then followed by a pronounced emission increase phase with time (Fig. 2C and 3C), which is virtually coincident with the late growth phase of fibril formation. This transition is reproducible in our experiments. The fluorescence intensity of the Phe_{CN}4 residue in $A\beta_{1-23}$M4 remains almost constant during the experimental period (Fig. 2D and 3D) and is consistent with its aforementioned weak aggregation propensity.

The site-specific assessment of $A\beta_{1-23}$ aggregation demonstrates distinct local dynamics during its aggregation process. For instance, the adjacent residues, Phe19 and Phe20, experience different environmental changes as time progresses. The decrease in

fluorescence intensity of Phe_{CN} in the $A\beta_{1-23}M2$ and M3 mutants starts prior to the onset of fibril formation. Accordingly, we reasonably speculate that the central hydrophobic core "LVFFA" (residues 17-21), crucial for the formation and stabilization of fibrillar structure of $A\beta_{1-40}/A\beta_{1-42}$,[14] also plays an essential role in the formation of the nucleating intermediates of $A\beta_{1-23}$. The formation of the nucleus likely favors a conformation wherein the Phe19 and Phe20 residues at this region are embedded in hydrophobic clusters, resulting in the Phe_{CN} fluorescence drop. A presumed subsequent nucleated conformational conversion process,[15] followed by elongation to form ordered antiparallel β-sheet structure, may place the Phe20 residue in a much less hydrophobic environment. This is indicated by the pronounced increase of the $Phe_{CN}20$ fluorescence intensity (Fig. 3C). On the basis of the experimental results, a preliminary plausible aggregation model of $A\beta_{1-23}$ is proposed in Fig. 4, and a favorable antiparallel alignment of β-sheet in fibrils is represented. Future experiments using high resolution techniques, such as NMR, will be expected to directly test and validate the β-sheet strucuture proposed in this model. Here, as proposed in this model, the mature fibrils are composed of in-register β-strands that flip over and pack with a neighboring molecular unit in an antiparallel orientation. The Phe20 residue, in this structure, is located in a highly polar environment, surrounded by Asp1, Glu3, and Arg5 residues from the adjacent strands (Fig. 4). This possibly favors its hydration and hydrogen bond formation, which would account for the increase in the $Phe_{CN}20$ fluorescence at the late phase of peptide aggregation.[5c, 9b, 13]

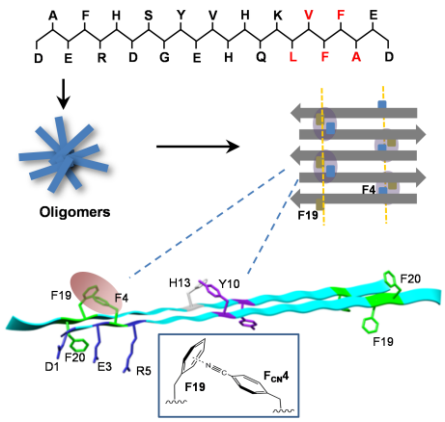

Fig. 4 A schematic representation of the $A\beta_{1-23}$ aggregation process and a proposed antiparallel packing topology between adjacent in-register β-strands in fibrils. The proposed perturbation of the Phe19-Phe4 aromatic interaction caused by substitution of Phe4 with $Phe_{CN}4$ residue is illustrated in the box.

The side chain of Phe19 is placed on the opposite side of the plane of the in-register β-strands in fibrils, in contrast to the adjacent Phe20 residue. The intensity of $Phe_{CN}19$ in $A\beta_{1-23}M2$ gradually decreases with time until mature fibrils form (Fig. 3B), suggesting a putative gradual transfer of the residue from a polar and solvent accessible environment to a more hydrophobic environment during aggregation. In the fibrillar structure, this residue is likely surrounded by a local nonpolar environment formed by the Leu17 and Ala21 residues on the same strand, and the Ala2 and Phe4 residues from the adjacent strands (Fig. 4).

To further verify the local conformational differences of the residues at amino acid positions 19 and 20, we performed Raman spectroscopy on the $A\beta_{1-23}M2$ and $A\beta_{1-23}M3$ mutants. The CN stretching band is strongly dependent on the polarity of its environment.[7a, 16] For example, in H_2O, the CN stretching vibrational band of Phe_{CN} is centered at ~2237 cm^{-1}, whereas this band shifts to ~2229 cm^{-1} in less polar solvents.[7a, 16b] Here, we employed the drop coating deposition Raman method, which provides high detection sensitivity while the peptide sample remains partially hydrated and largely retains its solution structure.[17] As shown in Fig. 5, the CN band of freshly prepared $A\beta_{1-23}M2$ and $A\beta_{1-23}M3$ is centered at 2237 cm^{-1}. This is similar to what was observed for the aqueous solutions of the free Phe_{CN} amino acid and Phe_{CN}-substituted mastoparan X peptide.[16b] This suggests that the $Phe_{CN}19$ in $A\beta_{1-23}M2$ and the $Phe_{CN}20$ in $A\beta_{1-23}M3$ are both well exposed to the solvent in a freshly prepared peptide solution. After three days of incubation, $A\beta_{1-23}M2$ exhibits a strong CN stretching band peaking at 2229 cm^{-1} (Fig. 5). The significant peak shift of 8 cm^{-1} to a lower wavenumber upon aggregation suggests a shift to a more hydrophobic and less solvent accessible environment for the CN probe in the fibrillar structure.[16b] In contrast, the CN band of the $A\beta_{1-23}M3$ aggregates appears at a higher frequency of 2235 cm^{-1}. There is only a 2 cm^{-1} red shift of the peak upon aggregation, much less than that of $A\beta_{1-23}M2$. This clearly demonstrates a much more polar local environment of $Phe_{CN}20$ in fibrils in comparison to the $Phe_{CN}19$ residue. The Raman results further corroborate our fluorescent results, strongly indicating distinct local environment changes of these two adjacent residues over the course of peptide aggregation.

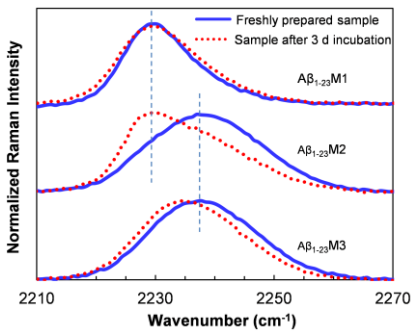

Fig. 5 Raman spectra of $A\beta_{1-23}M1$-M3 before and after being incubated for 3 d. The samples (2 mM) were incubated in 50 mM phosphate buffer of pH 7.4 at 25 °C. The vertical dashed lines indicate Raman wavenumbers at 2229 and 2237 cm^{-1}, respectively.

The remarkable disruption of fibril formation by replacing Phe4 to Phe_{CN} indicates the critical role of the Phe4 side chain in the formation of cross-β-sheet structure of fibrils, in accord with our proposed model. As depicted in Fig. 4, Phe4 and Phe19 from the adjacent intermolecular strands are on the same side of the plane of in-register β-strands and in close proximity to interact with each other. More specifically, on the basis of the strong perturbing effect of the CN group in $Phe_{CN}4$, we reasonably speculate the formation of a T-shaped edge-to-face aromatic interaction between these two residues (Fig. 4). Interactions of the aromatic residues could provide an energetic contribution as well as directionality and orientation that are facilitated by the restricted geometry of the planar aromatic ring,[10a, 18] thus contributing to the stabilization of β-sheets. The presence of the para-CN group on the side chain of $Phe_{CN}4$ derivative induces a van der Waal's repulsion which is energetically unfavorable as the CN group in $Phe_{CN}4$ directly faces the center of Phe19 (Fig. 4).[19] Moreover, the addition of a para-CN at Phe4 leads to a potential steric hindrance which also interferes with the Phe4-Phe19 interaction. These facts should account for the significantly decreased aggregation propensity of $A\beta_{1-23}M4$. Substitution of Phe19 with Phe_{CN} in $A\beta_{1-23}M2$ also slows down the aggregation rate, which corroborates our hypothesis. In this case, the CN group in $Phe_{CN}19$ would be oriented away from Phe4, which minimizes the

steric component, unlike in $A\beta_{1-23}M4$. Therefore, $A\beta_{1-23}M2$ still aggregates, but with a slower speed compared to the wild type $A\beta_{1-23}$. These results are in agreement with previous reports that the presence of an electron-withdrawing CN group on the facial ring of edge-to-face benzenes increases interaction energies, thus destabilizing the aromatic stacking.[20]

The fast decrease of $Phe_{CN}10$ fluorescence in $A\beta_{1-23}M1$ suggests that other hydrophobic residues, e.g., the "SGY" (residues 8-10) region, may also contribute to the early oligomerization process. Upon the formation of amyloids, there is a ~ 70% drop of the initial Phe_{CN} fluorescence intensity. This most significant drop might be because of the tight packing of the central residual region in oligomers and fibrils, thus minimizing the solvent accessibility. In Raman spectroscopy studies, a clear peak at 2237 cm^{-1} was not observable for the $A\beta_{1-23}M1$ fresh sample; instead we observed a lower frequency CN stretching band centered at 2229 cm^{-1} (Fig. 5). The band position shows almost no change after three days of incubation. This suggests that the residue at position 10 is quickly sequestered in a less solvent accessible environment, possibly due to the fast aggregation rate of $A\beta_{1-23}M1$ at a high concentration regime. Finally, we observed that the $Phe_{CN}10$ steady state fluorescence anisotropy increases upon aggregation of $A\beta_{1-23}M1$ (Fig. S9). In addition, the average lifetime of $Phe_{CN}10$ residue in $A\beta_{1-23}M1$ also increases from ~ 3.39 ns to ~ 4.36 ns upon aggregation (Fig. S10). A triple-exponential function is used to satisfactorily fit the fluorescence decay of the samples. This possibly indicates the heterogeneity of the microenvironment of the residue.[5g, 13]

In conclusion, we have characterized distinct site-specific dynamics of $A\beta_{1-23}$ amyloidogenesis using Phe_{CN} as both a fluorescent and Raman probe. Our results demonstrate that the Phe19 and Phe20 residues are both embedded in a hydrophobic core environment in oligomeric intermediates, whereas the subsequent conformational rearrangement of the strands toward fibril formation places Phe20 in a more polar environment, in comparison to that of Phe19. Furthermore, our results indicate the critical role of an edge-to-face aromatic interaction between the Phe4 and Phe19 residues on the adjacent in-register β-strands in facilitating the self-assembly and stabilizing the fibrillar structure. The residual alignment in the antiparallel β-sheet pattern is also proposed on the basis of the Phe_{CN} probing results. In light of the high sensitivity and fast time resolution of the Phe_{CN} optical probe, we envision that this approach, in combination with other methods including molecular dynamics simulation, will be valuable for illuminating local mechanistic details of oligomerization and fibrillization of a variety of *de novo* designed or directly disease-related amyloidogenic proteins.

D.D. and E.P.W. thank Florida Atlantic University for supporting this research. R.O. thanks the FOPI UPRH Program for supporting this research.

Notes and references

[a] Department of Chemistry and Biochemistry, Florida Atlantic University, Boca Raton, FL 33431, USA. E-mail: ddu@fau.edu
[b] Department of Chemistry, University of Puerto Rico-Humacao, Humacao, Puerto Rico 00791, Puerto Rico.
[c] Department of Chemistry and Biochemistry, Florida International University, Miami, FL 33199, USA.
[d] Department of Biomedical Science, Florida Atlantic University, Boca Raton, FL 33431, USA.

Electronic Supplementary Information (ESI) available: experimental methods, aggregation kinetics, AFM images, anisotropy and lifetime results, infrared spectra of $A\beta_{1-23}$ mutants. See DOI: 10.1039/c000000x/

1 (a) D. J. Selkoe, *Nature*, 2003, **426**, 900; (b) F. Chiti and C. M. Dobson, *Annu. Rev. Biochem.*, 2006, **75**, 333.
2 (a) C. Ritter, M. L. Maddelein, A. B. Siemer, T. Luhrs, M. Ernst, B. H. Meier, S. J. Saupe and R. Riek, *Nature*, 2005, **435**, 844; (b) J. X. Lu, W. Qiang, W. M. Yau, C. D. Schwieters, S. C. Meredith and R. Tycko, *Cell*, 2013, **154**, 1257.
3 C. Haass and D. J. Selkoe, *Nat. Rev. Mol. Cell Biol.*, 2007, **8**, 101.
4 (a) I. Mikhalyov, A. Olofsson, G. Gröbner and L.-Å. Johansson, *Biophys. J.*, 2010, **99**, 1510; (b) S. D. Quinn, P. A. Dalgarno, R. T. Cameron, G. J. Hedley, C. Hacker, J. M. Lucocq, G. S. Baillie, I. D. Samuel and J. C. Penedo, *Mol. Biosyst.*, 2014, **10**, 34; (c) J. C. Lee, R. Langen, P. A. Hummel, H. B. Gray and J. R. Winkler, *Proc. Natl. Acad. Sci. U. S. A.*, 2004, **101**, 16466.
5 (a) J. K. Chung, M. C. Thielges and M. D. Fayer, *J. Am. Chem. Soc.*, 2012, **134**, 12118; (b) J. Zimmermann, M. C. Thielges, Y. J. Seo, P. E. Dawson and F. E. Romesberg, *Angew. Chem. Int. Ed. Engl.*, 2011, **50**, 8333; (c) M. J. Tucker, R. Oyola and F. Gai, *Biopolymers*, 2006, **83**, 571; (d) J. Tang, H. Yin, J. Qiu, M. J. Tucker, W. F. DeGrado and F. Gai, *J. Am. Chem. Soc.*, 2009, **131**, 3816; (e) M. J. Tucker, R. Oyola and F. Gai, *J. Phys. Chem. B*, 2005, **109**, 4788; (f) K. N. Aprilakis, H. Taskent and D. P. Raleigh, *Biochemistry*, 2007, **46**, 12308; (g) A. L. Serrano, O. Bilsel and F. Gai, *J. Phys. Chem. B*, 2012, **116**, 10631.
6 I. T. Suydam, C. D. Snow, V. S. Pande and S. G. Boxer, *Science*, 2006, **313**, 200.
7 (a) Z. Getahun, C. Y. Huang, T. Wang, B. De Leon, W. F. DeGrado and F. Gai, *J. Am. Chem. Soc.*, 2003, **125**, 405; (b) B. A. Lindquist and S. A. Corcelli, *J. Phys. Chem. B*, 2008, **112**, 6301; (c) M. M. Waegele, R. M. Culik and F. Gai, *J. Phys. Chem. Lett.*, 2011, **2**, 2598.
8 (a) H. Taskent-Sezgin, J. Chung, V. Patsalo, S. J. Miyake-Stoner, A. M. Miller, S. H. Brewer, R. A. Mehl, D. F. Green, D. P. Raleigh and I. Carrico, *Biochemistry*, 2009, **48**, 9040; (b) H. Taskent-Sezgin, P. Marek, R. Thomas, D. Goldberg, J. Chung, I. Carrico and D. P. Raleigh, *Biochemistry*, 2010, **49**, 6290; (c) J. M. Glasscock, Y. Zhu, P. Chowdhury, J. Tang and F. Gai, *Biochemistry*, 2008, **47**, 11070; (d) S. J. Miyake-Stoner, A. M. Miller, J. T. Hammill, J. C. Peeler, K. R. Hess, R. A. Mehl and S. H. Brewer, *Biochemistry*, 2009, **48**, 5953; (e) M. J. Tucker, J. Tang and F. Gai, *J. Phys. Chem. B*, 2006, **110**, 8105; (f) D. Du, H. Liu and B. Ojha, *Methods Mol. Biol.*, 2013, **1081**, 77.
9 (a) P. Marek, R. Gupta and D. P. Raleigh, *ChemBioChem*, 2008, **9**, 1372; (b) P. Marek, S. Mukherjee, M. T. Zanni and D. P. Raleigh, *J. Mol. Biol.*, 2010, **400**, 878; (c) H. Inouye, K. A. Gleason, D. Zhang, S. M. Decatur and D. A. Kirschner, *Proteins*, 2010, **78**, 2306.
10 (a) R. Azriel and E. Gazit, *J. Biol. Chem.*, 2001, **276**, 34156; (b) J. J. Balbach, Y. Ishii, O. N. Antzutkin, R. D. Leapman, N. W. Rizzo, F. Dyda, J. Reed and R. Tycko, *Biochemistry*, 2000, **39**, 13748; (c) M. Grabenauer, C. Wu, P. Soto, J.-E. Shea and M. T. Bowers, *J. Am. Chem. Soc.*, 2009, **132**, 532.
11 D. Du, A. N. Murray, E. Cohen, H. E. Kim, R. Simkovsky, A. Dillin and J. W. Kelly, *Biochemistry*, 2011, **50**, 1607.
12 (a) C. Lee and M. Cho, *J. Phys. Chem. B*, 2004, **108**, 20397; (b) W. H. Moore and S. Krimm, *Proc. Natl. Acad. Sci. U. S. A.*, 1975, **72**, 4933.
13 A. L. Serrano, T. Troxler, M. J. Tucker and F. Gai, *Chem. Phys. Lett.*, 2010, **487**, 303.
14 (a) A. D. Williams, S. Shivaprasad and R. Wetzel, *J. Mol. Biol.*, 2006, **357**, 1283; (b) B. Urbanc, L. Cruz, S. Yun, S. V. Buldyrev, G. Bitan, D. B. Teplow and H. E. Stanley, *Proc. Natl. Acad. Sci. U. S. A.*, 2004, **101**, 17345.
15 (a) J. Lee, E. K. Culyba, E. T. Powers and J. W. Kelly, *Nat. Chem. Biol.*, 2011, **7**, 602; (b) T. R. Serio, A. G. Cashikar, A. S. Kowal, G. J. Sawicki, J. J. Moslehi, L. Serpell, M. F. Arnsdorf and S. L. Lindquist, *Science*, 2000, **289**, 1317; (c) K. Garai and C. Frieden, *Proc. Natl. Acad. Sci. U. S. A.*, 2013, **110**, 3321.
16 (a) I. T. Suydam and S. G. Boxer, *Biochemistry*, 2003, **42**, 12050; (b) C. L. Weeks, A. Polishchuk, Z. Getahun, W. F. Degrado and T. G. Spiro, *J. Raman Spectrosc.*, 2008, **39**, 1606.
17 C. Ortiz, D. Zhang, Y. Xie, A. E. Ribbe and D. Ben-Amotz, *Anal. Biochem.*, 2006, **353**, 157.
18 T. J. Smith, C. I. Stains, S. C. Meyer and I. Ghosh, *J. Am. Chem. Soc.*, 2006, **128**, 14456.
19 (a) F. R. Fischer, W. B. Schweizer and F. Diederich, *Chem. Commun.*, 2008, 4031; (b) E.-i. Kim, S. Paliwal and C. S. Wilcox, *J. Am. Chem. Soc.*, 1998, **120**, 11192.
20 E. C. Lee, B. H. Hong, J. Y. Lee, J. C. Kim, D. Kim, Y. Kim, P. Tarakeshwar and K. S. Kim, *J. Am. Chem. Soc.*, 2005, **127**, 4530.

Table of Contents:

Using an unnatural amino acid *p*-cyanophenylalanine as a both fluorescent and Raman probe, we characterized distinct local environmental changes of specific residues along the aggregation pathway of $A\beta_{1\text{-}23}$, and inferred a critical edge-to-face aromatic interaction for forming and stabilizing β-sheet structure.